

Microlensing and the Stellar Mass Function

Andrew Gould¹

Dept of Astronomy, Ohio State University, Columbus, OH 43210

e-mail gould@payne.mps.ohio-state.edu

Abstract

Traditional approaches to measuring the stellar mass function (MF) are fundamentally limited because objects are detected based on their luminosity, not their mass. These methods are thereby restricted to luminous and relatively nearby stellar populations. Gravitational microlensing promises to revolutionize our understanding of the MF. It is already technologically feasible to measure the MFs of the Galactic disk and Galactic bulge as functions of position, although the actual execution of this program requires aggressive ground-based observations including infrared interferometry, as well as the launching of a small satellite telescope. Rapid developments in microlensing, including the new technique of “pixel lensing” of unresolved stars, will allow one to probe the MF and luminosity function of nearby galaxies. Such observations of M31 are already underway, and pixel-lensing observations of M87 with the *Hubble Space Telescope* would permit detection of dark intra-cluster objects in Virgo. Microlensing techniques can also be applied to investigate the star-formation history of the universe and to search for planets with masses as small as the Earth’s.

Based on an invited talk at the January 1996 AAS meeting in San Antonio.

PASP (June 1996) in press, (c) ASP, reproduced with permission.

¹ Alfred P. Sloan Foundation Fellow

1. Introduction

Few would argue with the assertion that the best way to find out about stars is to observe them. However, while this traditional approach has been and continues to be very successful, it does have its limitations. To be observed, a star must be luminous enough and close enough to be detected. This obviously creates a heavy selection bias toward brighter stars. It is generally possible to quantify and compensate for this bias. Nevertheless, as stars get sufficiently faint, the available volume becomes so small that the statistics are compromised. Below the hydrogen-burning limit ($M \sim 0.08 M_{\odot}$), the luminosity of the star (or rather brown dwarf) depends not only on its mass but also its age. The age in turn is strongly correlated with position; younger objects are confined close to the Galactic plane and older ones are distributed at greater heights. For these reasons, our ability to probe the stellar mass function (MF) breaks down rapidly as one approaches and then crosses the hydrogen-burning limit.

Other problems emerge if we try to measure the MF at locations other than the immediate solar neighborhood. First, of course, it becomes increasingly difficult to detect faint stars. However, there is a more fundamental problem. The masses of individual stars are estimated with the help of a mass-luminosity relation, where the luminosity is given in some observed band such as V or K . This relation is in turn calibrated using stars in (e.g. visual) binaries whose masses are well determined. Since the distances (and so absolute magnitudes) are also well determined, the calibration is purely empirical. Unfortunately, it is also purely local. The mass-luminosity relation may depend on location through metallicity, age, or other factors. It is impossible to measure the MF in a region far from the solar neighborhood without a direct measurement of the mass of at least some stars in that region.

Microensing offers another approach. Microensing occurs when an object (“the lens”) comes close to the line of sight between the observer and a distant star (“the source”). The gravity of the lens deflects and thereby magnifies the light from the source. As the lens moves closer and then farther from the line of sight, the magnification rises from unity to some maximum value and then declines symmetrically. This characteristic one-time variation is then the signature of microensing.

The major advantage of microensing over traditional methods of measuring the MF is obvious: the microensing effect is produced by the mass of the lens, not its luminosity. Hence, microensing-selected samples are completely free of bias induced by the hydrogen-burning limit. Moreover, microlenses need not be nearby. The method can be used to probe the MF in remote regions of the Milky Way and even in other galaxies.

On the other hand, it is not at all obvious how one might go about measuring the mass of a lens once it is detected. Microlensing experiments were initially suggested as a method to detect Massive Compact Halo Objects (MACHOs) in the Milky Way halo by observing millions of source stars in the Large Magellanic Cloud (LMC) (Paczynski 1986). They were not expected to yield information about the mass of individual lenses to better than a factor ~ 3 . Rather, the goal was to measure the total mass in MACHOs and to make a rough estimate of the MACHO mass scale. Two groups have undertaken MACHO searches, MACHO (Alcock et al. 1993, 1995b, 1995d, 1996a) and EROS (Aubourg et al. 1993, 1995; Ansari 1996).

However, several developments have now combined to open the way to microlensing measurements of the MF. Paczynski (1991) and Griest et al. (1991) independently suggested that microlensing experiments toward the Galactic bulge could be used to probe stars along the line of sight in the Galactic disk. The OGLE (Udalski et al. 1994a, 1994b), MACHO (Alcock et al. 1995a, 1996b), and DUO (Alard, Mao, & Guibert 1995; Alard 1996) collaborations have all initiated such searches and the EROS collaboration plans to join them soon. A new Japan-New Zealand collaboration MOA is also actively preparing for observations. Kiraga & Paczynski (1994) pointed out that these searches are sensitive to stars in the Galactic bulge as well as the disk. Theoretical work by many people has shown that it is possible to recover far more information about individual masses than was originally believed. Crots (1992) and Baillon et al. (1993) developed “pixel lensing” techniques for finding lensing events of unresolved stars and applied them to observations of M31, thus creating the possibility of measuring the MF in external galaxies. Several of the microlensing collaborations have developed the ability to recognize ongoing events in real time. These “alert” events are now being followed by at least two world-wide networks, PLANET (Albrow et al. 1996) and GMAN (Pratt et al. 1996) with the aim of finding several classes of higher order effects predicted by theorists, including signatures of planets.

In brief, microlensing research is proceeding at an explosive pace. Paczynski (1996) and Roulet & Mollerach (1996) have given comprehensive reviews of these developments. Schneider, Ehlers, & Falco (1992) place microlensing in the broad context of other forms of gravitational lensing. Here the focus is on what microlensing can tell us about stars.

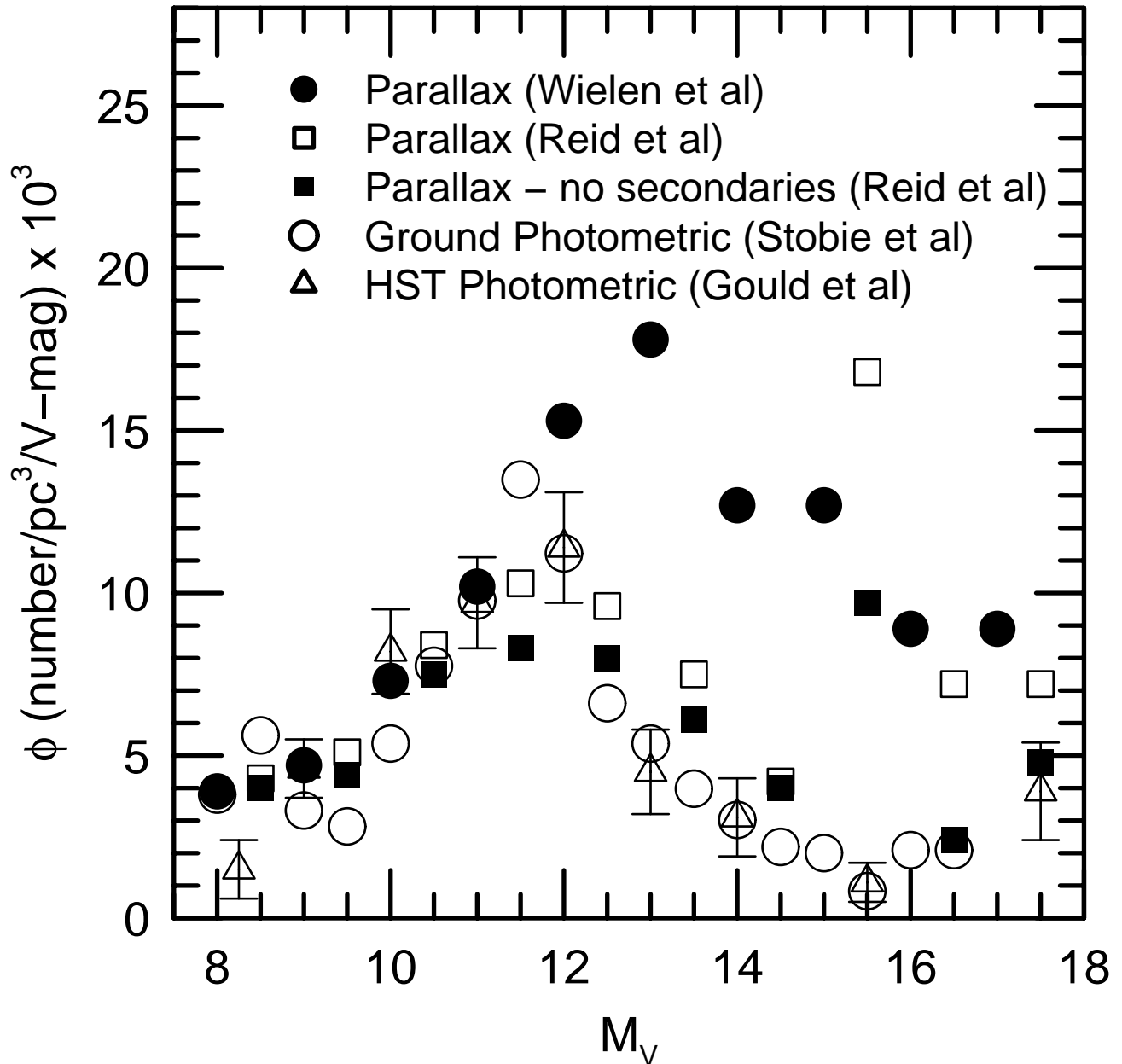


Figure 1. Luminosity function of disk stars as determined from *HST* data by Gould et al. (1996) (triangles) compared to several other determinations. Shown are the ground-based photometric survey of Stobie et al. (1989) (open circles), the parallax-star survey of Wielen et al. (1983) (filled circles) and the parallax-star study of Reid et al. (1995) excluding (filled squares) and including (open squares) the secondaries in binaries. Error bars are shown only for the *HST* data to avoid cluttering. Note that the photometric studies of Gould et al. and Stobie et al. are in almost perfect agreement. Also note from the Reid et al. data that about half of faint M stars are secondaries. From Gould et al. (1996). Copyright American Astronomical Society, reproduced with permission.

2. *HST* Star Counts

Star counts with the *Hubble Space Telescope* (*HST*) (Bahcall et al. 1994; Gould, Bahcall & Flynn 1996) provide a good illustration of both the recent progress

and fundamental limitations of traditional techniques. On the one hand, *HST* observations allow one to measure the luminosity function (LF) of M dwarfs up to several kpc from the Sun. These data have helped resolve a major conflict about the faint end of the LF which had persisted for more than 10 years. Photometric surveys of stars within ~ 100 pc (e.g. Stobie, Ishida, & Peacock 1989) have tended to show a sharply falling LF for stars $M_V > 12$, while in their more nearby parallax-based survey, Wielen, Jahreiss, & Krüger (1983) find a nearly flat LF.

There are important differences between the two types of surveys. In photometric surveys, one estimates the absolute magnitude of the star from the measured color and a local, empirically calibrated color-magnitude relation. The distance is then determined by comparing the absolute and apparent magnitudes. This method creates a statistical bias toward including brighter-than-average stars in the sample, called Malmquist bias, because the brighter stars can be detected over a larger volume. It is possible to correct for Malmquist bias, but this correction can be uncertain. In parallax surveys, by contrast, the distance is known from the parallax, and so the absolute magnitude is determined rather than estimated. On the other hand, of course, parallax surveys are limited statistically by the small volume probed.

The *HST* photometric survey has a mean limiting magnitude of $I = 23.7$, about 100 times fainter than is typical of ground-based surveys. It agrees almost perfectly with the Stobie et al. photometric survey. This shows first that the LF at a few kpc from the Sun is the same as the LF at ~ 100 pc. Moreover, since the *HST* observations reach to the “top” of the Galactic disk, they require only a modest correction for Malmquist bias. Hence their agreement with the more Malmquist-bias prone local sample is reassuring. The conflict between the photometric and parallax LFs has been significantly softened by the work of Reid, Hawley, & Gizis (1995), who made substantial new observations of parallax stars and did a thorough reanalysis of the data. They find that if one includes only single stars and the primaries of binaries (which is essentially all that photometric surveys detect), there is very good agreement between the photometric and parallax surveys. If the secondaries of binaries are re-included, then the luminosity function still falls, but not as rapidly as the photometric surveys would indicate (see Fig. 1). Thus, substantial progress has been made on the LF on several fronts.

The MF constructed by Gould et al. (1996) from the *HST* LF and the mass-luminosity relation of Henry & McCarthy (1993) falls for $M < 0.45 M_\odot$ ($M < 0.23 M_\odot$ if number density is measured per unit mass instead of log-mass). See Figure 2. The *HST* counts yield a number of other important results as well. The vertical distribution of M stars is measured for the first time. The intermediate component (“thick disk”) has a scale height $h \sim 660$ pc, much smaller than usually

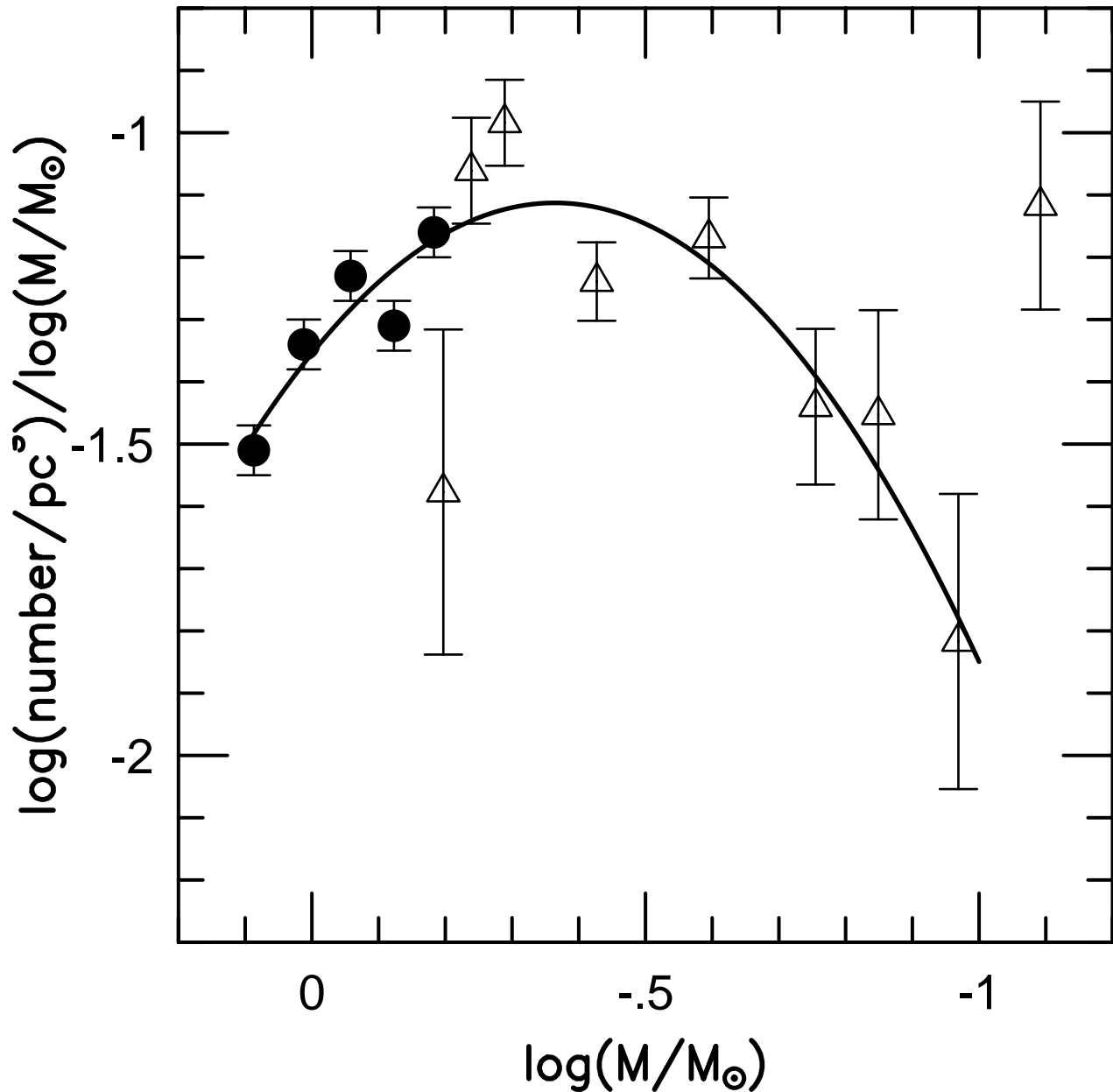


Figure 2. Mass function derived from luminosity functions of Gould et al. (1996) for $M_V > 8$ (triangles) and of Wielen et al. (1983) for $M_V < 8$ as shown in Fig. 1. Curve is a parabolic fit to the data excluding the last point. From Gould et al. (1996). Copyright American Astronomical Society, reproduced with permission.

assumed. The thin disk is inconsistent with an exponential profile (which is usually assumed) and is much closer to a sech^2 law. The total column density of M stars is only $\sim 13 M_{\odot} \text{pc}^{-2}$, implying that the observed column density of the disk is only $\Sigma \sim 40 M_{\odot} \text{pc}^{-2}$, about 20% less than the best previous estimate. Thus, the *HST* star counts provide a good example (certainly not the only one) of continuing advances in the study of stars by traditional techniques. Bessel & Stringfellow (1993) give a good recent review of the traditional approaches to this problem. See

also Scalo (1986).

On the other hand, Figures 1 and 2 also make clear the limitations of these techniques. First, of course, the graphs simply end at the hydrogen burning limit. Even the approach to the hydrogen limit is unclear. The *HST* data appear to show a rise at the last point, but this is based on only six stars and so is not significant. There are several intriguing lines of argument that the MF is rising at this point, including circumstantial evidence that young (and so more luminous) brown dwarfs are being detected and mistaken for faint stars (Reid, Tinney, & Mould 1994; Kirkpatrick et al. 1994). However, these results are based on only 17 detections and are open to conflicting interpretations. In brief, new approaches are needed to supplement the old.

3. Simple Microlensing

Consider a point mass M and a point source of light which are approximately aligned at distances D_1 and D_s from the observer. General relativity predicts that, in the weak field limit, the mass (the “lens”) deflects light by an angle α ,

$$\alpha = \frac{4GM}{bc^2}, \quad (3.1)$$

where b is the impact parameter (distance of closest approach) and where it is assumed that $b \ll D_1$, $b \ll D_{ls}$. Here $D_{ls} \equiv D_s - D_1$ is the distance from the lens to the source. The source will then be split into two images whose positions are governed by the equation

$$\theta_S^2 - \theta_I \theta_S + \theta_e^2 = 0, \quad (3.2)$$

where θ_S and θ_I are the angular separations between the lens and the source and image respectively, and where θ_e is the angular Einstein radius,

$$\theta_e \equiv \sqrt{\frac{4GM D_{ls}}{c^2 D_1 D_s}}. \quad (3.3)$$

Equation (3.2) has two solutions:

$$\theta_{I\pm} = \pm x_{\pm} \theta_e \quad (3.4)$$

where

$$x_{\pm} \equiv \frac{\sqrt{x^2 + 4} \pm x}{2}, \quad x \equiv \frac{\theta_S}{\theta_e}. \quad (3.5)$$

The (\pm) symbol indicates that two images are on opposite sides of the lens. The $(+)$ image has the larger separation and is on the same side as the source.

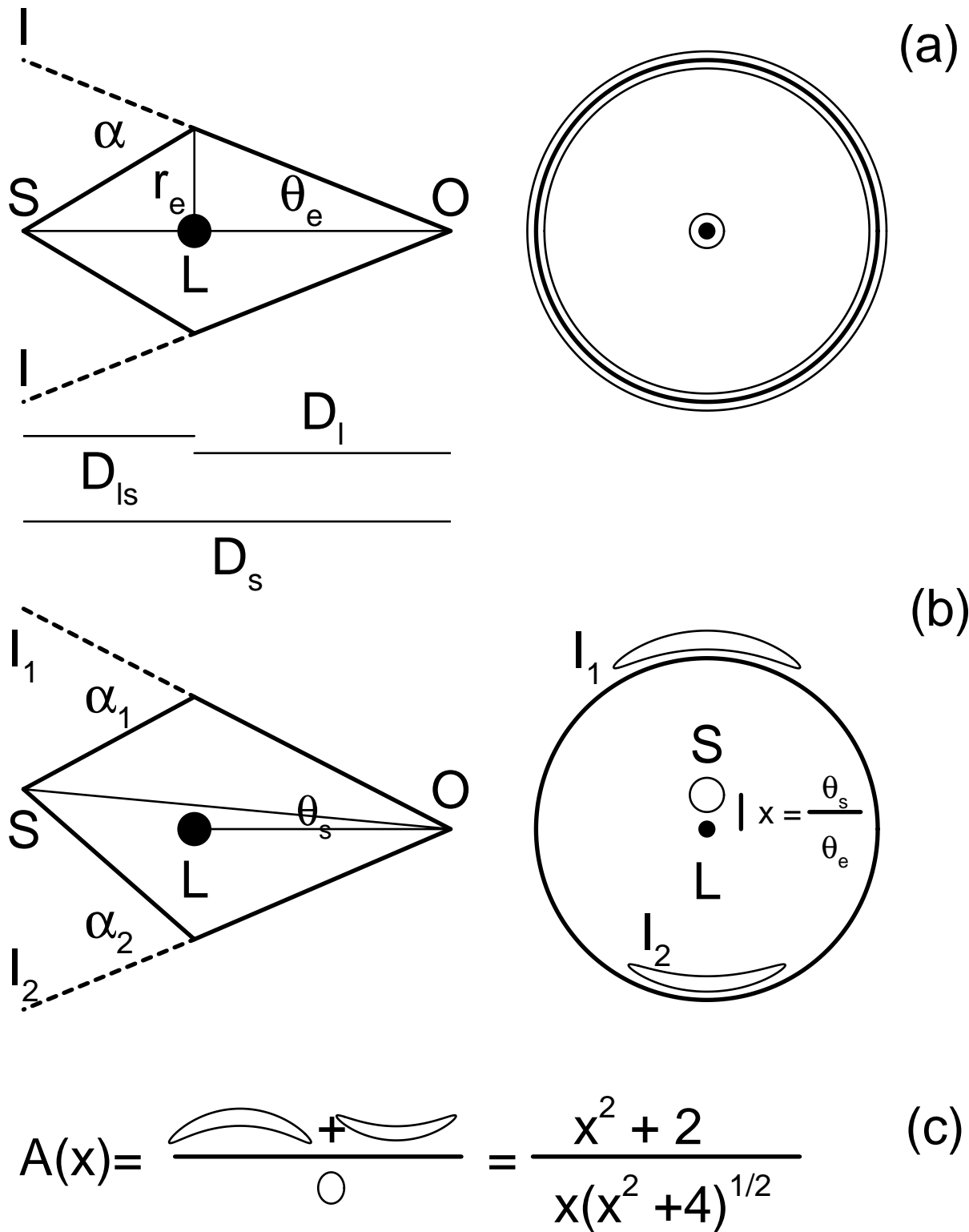


Figure 3. Geometry of Microlensing. Shown in (a) is the idealized case when the observer (O), the lens (L), and source (S) are perfectly aligned. Light from S is bent by an angle $\alpha = 4GM/r_e c^2$ [cf. eq. (3.1)] by the mass M of the lens. The image (I) is deflected by angle θ_e relative to the true source position. On the right the geometry is shown from the point of view of the observer. Again, the lens (solid circle) and source (small open circle) are perfectly aligned. The image is a ring of light (the “Einstein Ring”) between the two large non-bold circles which straddle the bold circle of angular radius θ_e . Shown in (b) is the more generic case where S and L are separated by a finite angle θ_s . There are now two different deflection angles α_1 and α_2 , one for each of the two images I_1 and I_2 . The images no longer make a ring, but it is still convenient to draw an imaginary Einstein ring (right). The brighter image falls outside the ring and the fainter image falls inside. Note that x is the separation of S and L in units of the Einstein ring. Shown in (c) is the magnification. The images have the same surface brightness as the source. Assuming the latter is uniform, the magnification is then simply the ratio of areas. Unless the lens transits the source, the magnification is given analytically by eq. (3.7).

Figure 3(a) illustrates this geometry for the special case when the lens is perfectly aligned with the source. Figure 3(b) shows the more typical case when the alignment is close, but not perfect.

Gravitational lenses, like telescope lenses, produce images which transform the size and shape of the source, but not the surface intensity of its light (Liouville 1837; Misner, Thorne, & Wheeler 1973). Thus for a source with uniform surface brightness, the magnification is given by the ratio of the areas of the images to the area of the source. This is shown in Figure 3(c). Each point of light from the source is stretched when it is mapped onto the images. From Figure 3(b) one sees that it is stretched by a factor x_{\pm}/x in the tangential direction, and by dx_{\pm}/dx in the radial direction. Hence the two images of a point source are magnified by,

$$A_{\pm}(x) = \left| \frac{x_{\pm}}{x} \frac{dx_{\pm}}{dx} \right| = \frac{x_{\pm}^2}{x_+^2 - x_-^2}, \quad (3.6)$$

yielding a total magnification,

$$A(x) = A_+ + A_- = \frac{x^2 + 2}{x\sqrt{x^2 + 4}}. \quad (3.7)$$

Unless the lens transits (or nearly transits) the source (see § 5.2), the magnification of a finite source is also very well approximated by equation (3.7). For typical microlensing events, $\theta_e \lesssim 1$ mas, which is not generally detectable. The magnification is therefore the only signature that a lensing event is in progress. However, as explained below, the magnification is not directly observable. What can be observed is the changing magnification as the lens moves on a straight line with projected separation from the source in units of the Einstein ring

$$x(t; t_0, \beta, \omega) = \sqrt{\omega^2(t - t_0)^2 + \beta^2}. \quad (3.8)$$

Here t_0 is the time of closest approach, β is the impact parameter in units of θ_e ,

$$\omega^{-1} \equiv t_e = \frac{r_e}{v} = \frac{D_1 \theta_e}{v}, \quad (3.9)$$

is the characteristic time scale of the event, $r_e \equiv D_1 \theta_e$ is the physical Einstein radius, and v is the speed of the lens relative to the Earth-source line of sight.

What is actually observed is the change in the flux of the source star

$$F(t; t_0, \beta, \omega, F_0) = \{A[x(t; t_0, \beta, \omega)] - 1\}F_0, \quad (3.10)$$

where F_0 is the unlensed flux of the star. (Note that F_0 is not known *a priori* from the pre-event light curve. What is measured before and after the event is

$F_0 + B$ where B is the sum of the fluxes from other non-lensed objects such as a binary companion, the lens itself, or random field stars. For most lensing events observed to date, the quality of the data has not been high enough to measure F_0 and B separately. Rather, the measured value of $F_0 + B$ is combined with a statistical estimate of B to obtain an estimate of F_0 . This statistical approach is certainly adequate for estimating the total density of dark objects, and blending is only a minor uncertainty in the results of MACHO and EROS. However, blending is a much more important problem when estimating the MF. See § 4. Direct measurements of F_0 which are free from blending corrections will be made in the future when high-quality data will be obtained from follow-up photometry. See § 5.2.)

Equation (3.10) immediately reveals the fundamental shortcoming of microlensing: even if the light curve is observed with perfect accuracy, it yields only four parameters: t_0 , β , ω , and F_0 . Of these four, only ω contains any information about the lens. Moreover, it is clear from equation (3.9) that ω is a complicated combination of the quantities one would like to know.

Faced with this difficulty, there are two options for using microlensing to learn about the MF of stars. First, make a statistical analysis of the measured time scales. As discussed in the next section, this approach requires assumptions about the velocity and space distributions of both the lenses and sources. Second, attempt to get more information so as to be able to measure the masses of individual lenses.

4. Initial Measurements of the Mass Function

Two groups have used the measured time scales of the first 51 events detected by MACHO and OGLE toward the bulge to attempt to determine the MF of the lensing stars along the line of sight in the disk and in the bulge itself (Zhao, Spergel, & Rich 1995; Han & Gould 1996a). See also Jetzer (1994). The results are subject to significant uncertainties, but are nonetheless striking. Han & Gould (1996a) considered three families of MFs: power law with cut off, Gaussian, and Hubble. The Hubble is the MF determined from the *HST* data by Gould et al. (1996), augmented by the observed density of white dwarfs.

The best fits are shown in Figure 4. The best fit power law, with a near-Salpeter slope of 2.1 and lower-mass cut off at $M = 0.04 M_\odot$, is preferred over the Hubble MF at $> 5\sigma$. (More formally, the χ^2 of the Hubble MF is greater than that of the best power law by $\chi_{\text{PL}}^2 - \chi_{\text{HST}}^2 = 5.5^2$.) The primary reason for the poor fit of the Hubble MF is that it fails to reproduce the short events. Thus, microlensing seems to be telling us that there are more low mass objects in either the disk or the bulge than are observed locally. One might be concerned that the Hubble MF

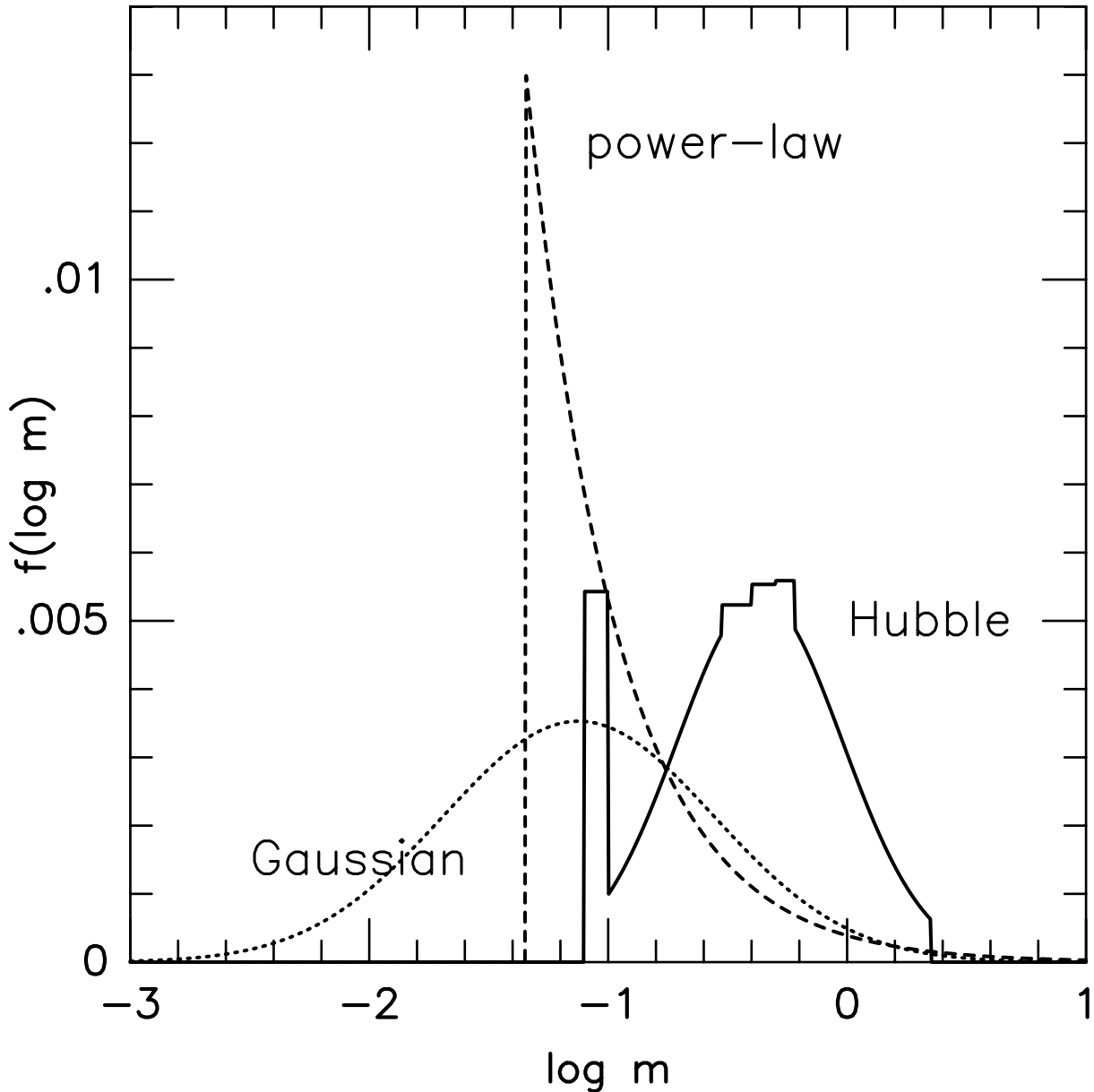


Figure 4. Best fit Gaussian and power-law mass functions determined by Han & Gould (1996a) from the first 51 microlensing events reported by MACHO and OGLE from observations toward the Galactic bulge. Also shown is the Hubble mass function as determined by Gould et al. (1996) from *HST* star counts (see Fig. 2) augmented to include the observed density of white dwarfs. The power law is favored over the Hubble at the 5.5σ level and over the Gaussian at the 3σ level. From Han & Gould (1996a). Copyright American Astronomical Society, reproduced with permission.

does not include the binary companions catalogued by Reid et al. (1995), but it is clear from a comparison between Figures 1 and 4 that this correction would not make a significant difference.

However, there are three problems with this approach which lessen one's confidence in the results. First, MACHO and OGLE determined the time scales assum-

ing that there is no blending [i.e., $B = 0$ in the discussion below eq. (3.10)]. If the events were in fact significantly blended, the true time scales would be longer than reported. Since the mass estimate scales $M \propto t_e^2$, the lower-mass cut off might be significantly underestimated. This problem will likely disappear as more events accumulate, particularly giant-source events (Gould 1995d) which are much less susceptible to blending. Second, the results are wholly dependent on the assumptions adopted for the velocity and spatial distributions of the lenses and sources. While the source distributions are reasonably well constrained by observations, the distributions of lenses must be inferred from the distributions of more luminous material. In fact, Zhao et al. (1995) used somewhat different distributions from those of Han & Gould (1996a) and got somewhat different results. However, the principal problem is that the mass of any given lens is very poorly constrained, so that (given the uncertainty in the lens velocities and positions) one will never obtain more than a crude picture of the mass spectrum, regardless of statistics. See for example the Gaussian versus power-law fits in Figure 4. If the preliminary detection of a large population of unseen low-mass objects is confirmed by continuing observations, then even such a crude determination would be quite important. However, the real interest would still be in obtaining detailed MFs for the disk and bulge separately.

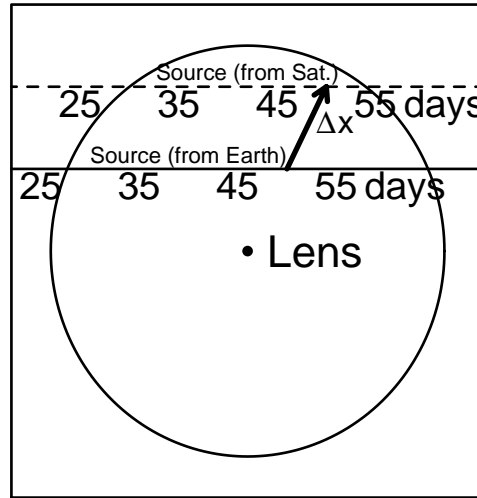
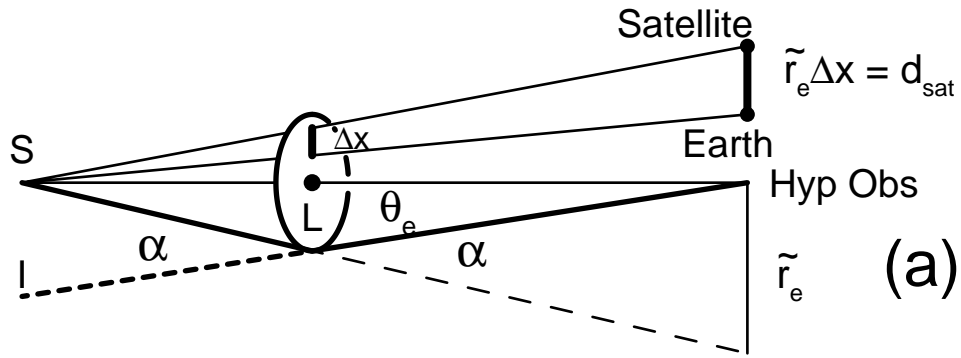
5. Mass Measurements of Individual Microlenses

Figure 5(a) is an elaboration of Figure 3(a), the Einstein ring diagram for a hypothetical observer perfectly aligned with the lens-source axis. The additional feature of this figure is \tilde{r}_e , the projection of the Einstein radius r_e onto the observer plane. The algebraic expression for the projected radius is $\tilde{r}_e = (D_s/D_{ls})r_e$, but its physical significance can be understood directly from Figure 5(a) which makes clear that knowledge of \tilde{r}_e , θ_e , and D_s would fix the distance to the lens, D_l . Then, from equation (3.3) one could determine M , and from equation (3.9) and the measured value of the time scale, t_e , one could determine v .

In fact, closer inspection of Figure 5(a) shows that M can be determined from \tilde{r}_e and θ_e , even if D_s is unknown. Using the small angle approximation (certainly valid for angles $\lesssim \text{mas}$), one sees from the diagram that $\alpha : \tilde{r}_e = \theta_e : r_e$, implying

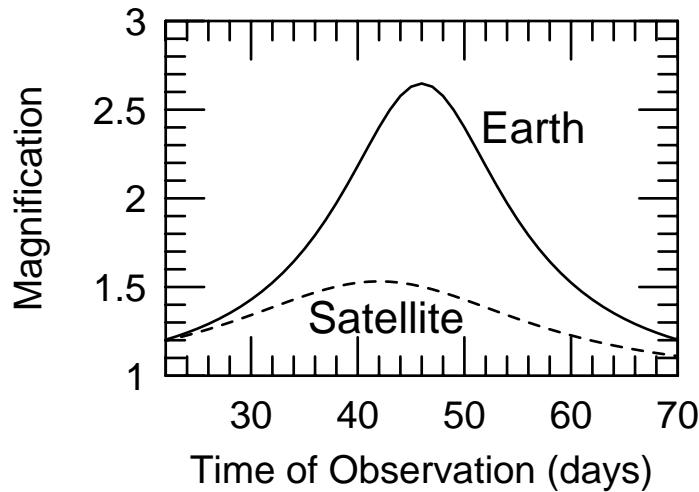
$$\theta_e \tilde{r}_e = \alpha r_e = \frac{4G}{c^2} M, \quad (5.1)$$

where in the last step I have made use of the Einstein light deflection equation (3.1).



$$\tilde{r}_e = \frac{d_{\text{sat}}}{\Delta x}$$

(b)



(c)

Figure 5. Geometry of microlensing parallax. Part (a) is an elaboration of the lensing geometry for a hypothetical observer perfectly aligned with the source-lens axis. As in Fig. 3(a), α is the bending angle and θ_e is the angular Einstein radius. The physical Einstein ring is the circle centered on L. Its radius, r_e , is not explicitly labeled. In addition, the diagram shows \tilde{r}_e , the projection of r_e onto the plane of the observer. Parts (b) and (c) show how \tilde{r}_e is measured by parallax. Part (b) shows the source position in the Einstein ring as a function of time (labeled in days) as seen from the Earth and satellite. The vector separation $\Delta \mathbf{x} = (\omega \Delta t, \Delta \beta)$ remains a constant during the event. The resulting light curves as seen from the Earth and satellite are shown in (c). By measuring the impact parameters β and β' and the times of maximum t_0 and t'_0 , one can reconstruct the geometry of (b) and so determine $\Delta \mathbf{x}$. From (a) it is clear that the magnitude of this vector, Δx , is the distance to the satellite d_{sat} as a fraction of \tilde{r}_e . One therefore recovers $\tilde{r}_e = d_{\text{sat}}/\Delta x$. The solution is actually degenerate because from the light curves (c) alone one cannot tell whether the source trajectories in (b) pass on the same or opposite sides of the lens. As discussed in the text, the degeneracy can be broken. Parts (b) and (c) adapted from Gould (1994b). Copyright American Astronomical Society, reproduced with permission.

Is it possible to measure the \tilde{r}_e and θ_e for a representative sample of events and so determine the MF? With some work, yes. Moreover, since D_s is typically known to $\sim 10\%$ for bulge sources, not only the mass, but also the approximate distance would be known. Hence one could determine the bulge and disk MFs separately.

5.1. PARALLAX SATELLITE MEASUREMENTS OF \tilde{r}_e

For galactic bulge sources at $D_s \sim R_0 = 8 \text{ kpc}$, $\tilde{r}_e = 8\sqrt{(M/M_\odot)D_l/D_{ls}}$ AU. Hence, if the event is observed from a satellite displaced from the Earth in the observer plane by $d_{\text{sat}} \sim \mathcal{O}(\text{AU})$, the event will look significantly different. It will have a different t_0 and a different β (Refsdal 1966; Gould 1994b). As shown in Figure 5(b-c), one can use the difference in the two light curves to reconstruct the separation in the Einstein ring $\Delta\mathbf{x}$,

$$\Delta\mathbf{x} = (\omega\Delta t, \Delta\beta), \quad (5.2)$$

where Δt and $\Delta\beta$ are the differences in the light-curve parameters as seen from the satellite and Earth. By measuring $\Delta\mathbf{x}$, one can determine \tilde{r}_e [see Fig. 5(a)],

$$\tilde{r}_e = \frac{d_{\text{sat}}}{\Delta x}. \quad (5.3)$$

In fact, the situation is not quite so simple. As portrayed in Figure 5(b), the source passes on the same side of the lens as seen from the Earth and the satellite. In this case $\Delta\beta = \Delta\beta_-$, where $\Delta\beta_\pm \equiv |\beta' \pm \beta|$ and β' is the impact parameter as seen from the satellite. But in fact, from the measurement of β and β' alone, one has no way of knowing whether the source is on the same or opposite side as seen by the two observers. For the opposite-side case $\Delta\beta = \Delta\beta_+$. Hence there are two possible solutions for $\tilde{r}_e = d_{\text{sat}}[(\omega\Delta t)^2 + (\Delta\beta_\pm)^2]^{-1/2}$. Fortunately, this degeneracy can be broken by measuring the fractional difference in time scales between the Earth and satellite, $\Delta\omega/\omega$, which arises from the relative motion of the Earth and satellite, v_{sat} . The larger the projected speed of the lens, $\tilde{v} \equiv \omega\tilde{r}_e$, is relative to v_{sat} , the smaller $\Delta\omega/\omega$. Hence, the time-scale difference allows one to choose the correct solution (Gould 1995a). Numerical simulations by Gaudi & Gould (1996) show that 2% photometry (which for bulge giant sources could be obtained using a $\sim 25 \text{ cm}$ telescope) would be adequate to measure \tilde{r}_e . The reason for focusing on giants will become clear in the next section.

It is possible in principle to use the Earth's orbital motion to measure parallax from the ground (Gould 1992), and in fact one such measurement has already been made (Alcock 1995c). However, for typical events the Earth does not change its velocity enough over the event time scale to produce a significant effect.

The primary motivation for launching a parallax satellite would be to determine the nature of the MACHOs now apparently being detected toward the LMC by MACHO and EROS (Alcock et al. 1993, 1995b, 1995d, 1996a, 1996c; Aubourg et al. 1993, 1995; Ansari et al. 1996). For these objects, measurement of \tilde{v} alone would distinguish among objects in the Galactic disk, Galactic halo, and LMC (Boutreux & Gould 1996). For lensing events seen toward the bulge, parallax observations do not by themselves provide such a clear cut distinction among populations, although they do help (Han & Gould 1995). However, for the bulge, unlike the LMC, it is possible to obtain a third piece of information, θ_e , for a representative subset of events.

5.2. MEASUREMENT OF θ_e

There are two classes of methods which have been proposed for measuring θ_e : those that work best when θ_e is small and those that work best when θ_e is large.

The first class of methods relies on the finite size of the source. If the lens transits or comes sufficiently close to the source, then the magnification will deviate from the point-source formula (3.7) (Gould 1994a; Nemiroff & Wickramasinghe 1994; Witt & Mao 1994). This can be seen most easily by considering the case of $x \rightarrow 0$ for which $A(x) \rightarrow x^{-1} \rightarrow \infty$. For simplicity consider a source with uniform surface brightness, since for these the magnification is just the area of the image divided by the area of the source. The image ring in Figure 3(a) appears to have a width about equal to the radius of the star, θ_* . In fact, one finds from equation (3.5) that the width is exactly θ_* . Hence the maximum magnification is given by

$$A_{\max} \sim \frac{2\pi\theta_e\theta_*}{\pi\theta_*^2} = 2\frac{\theta_e}{\theta_*}. \quad (5.4)$$

By frequently monitoring the event, one can identify the time (and hence the value of $x = x_*$) when the lens passes over the edge of the star. The value of θ_* can be determined from the star's measured temperature and Stefan's law. Hence, one can compute $\theta_e = x_*^{-1}\theta_*$.

For fixed θ_e and θ_* , the fraction of events with such transits is θ_*/θ_e . For an ensemble of source stars at the Galactic center ($R_0 = 8\text{kpc}$) with mean physical radius $\langle r_* \rangle$, the fraction is

$$\frac{\langle \theta_* \rangle}{\theta_e} = \frac{\langle r_* \rangle / R_0}{\theta_e} = \frac{13\mu\text{as}}{\theta_e} \frac{\langle r_* \rangle}{22r_\odot}, \quad (5.5)$$

where the normalization is relative to the mean radius of bulge giants, $\langle r_* \rangle \sim 22r_\odot$ (Gould 1995d) and r_\odot is the solar radius. Since the distribution of Einstein radii

is expected to peak at $\theta_e \sim 130 \mu\text{as}$ (see below), only $\sim 10\%$ of giant-source events yield measurements of θ_e . For the more common turn-off stars, the fraction is $\sim 1\%$. This is the principal (but not the only) reason why lensing searches should be tuned to finding giant-source events (Gould 1995d). Finite source effects have been observed in one “normal” microlensing event seen toward the bulge (Alcock et al. 1996d) as well as in two binary-lens events, one toward the bulge (Udalski et al. 1994c; Alcock et al. 1996b) and one toward the LMC (Alcock et al. 1996c).

It is in fact possible to about double the number of measurements relative to equation (5.5). If the lens passes close to the limb of the star but does not actually transit, there is still a noticeable change in the magnification relative to the point-source formula, $\delta A/A = \Lambda/8(x_*/x)^2$. Here Λ is the second radial moment of the stellar flux normalized so that $\Lambda = 1$ for a uniform disk. Unfortunately, if the lens does not transit the star, then this effect simply masquerades as a change in β , so it cannot actually be detected (Gould & Welch 1996). However, giant stars are limb darkened by different amounts in different spectral bands. If the star could be resolved, it would have a blue core and a red rim. This can give rise to color effects during the microlensing event because the lens magnifies the near part of the star more than the far part (Witt 1995). These color effects cannot be mimicked by a change in lensing parameters, since point-source lensing is achromatic. For the specific choice of V and H bands, Gould & Welch (1996) find $\Lambda^H - \Lambda^V = 0.07$, which implies a color shift of $\sim 0.01(x_*/x)^2$ mag. By aggressively monitoring giant star events with an optical/infrared camera equipped with a dichroic beam splitter, they estimate that θ_e could be measured for $\beta \leq 2x_*$. See also the related idea of Loeb & Sasselov (1995) to make use of Ca II limb brightening.

Figure 6 shows the expected distribution of θ_e based on the best-fit model of Han & Gould (1996a). The lower solid curve shows the fraction of giant source events for which measurement of θ_e is possible with optical/infrared photometry. The fraction is a respectable 20% at the peak of the curve, but falls drastically along the long tail toward larger θ_e . If measurements are to be made for a representative sample of events (which is essential to determining the MF), then some alternative method must be used for large θ_e . Several such methods have been proposed: direct imaging (Gould 1992), apparent proper motion of the mean image position (Hog, Novikov, & Polnarev 1995), and even lunar occultations (Han, Narayanan, & Gould 1996). The best prospect at the present time seems to be direct imaging using infrared interferometry.

The CHARA interferometer (McAlister et al. 1994, 1995) now under construction is expected to be able to resolve images separated by $0.6 (\lambda/1.65 \mu\text{m})$ mas at 13th magnitude. The magnitude limit forces one into the infrared because few lensing events are this bright in the optical, even when the sources are restricted

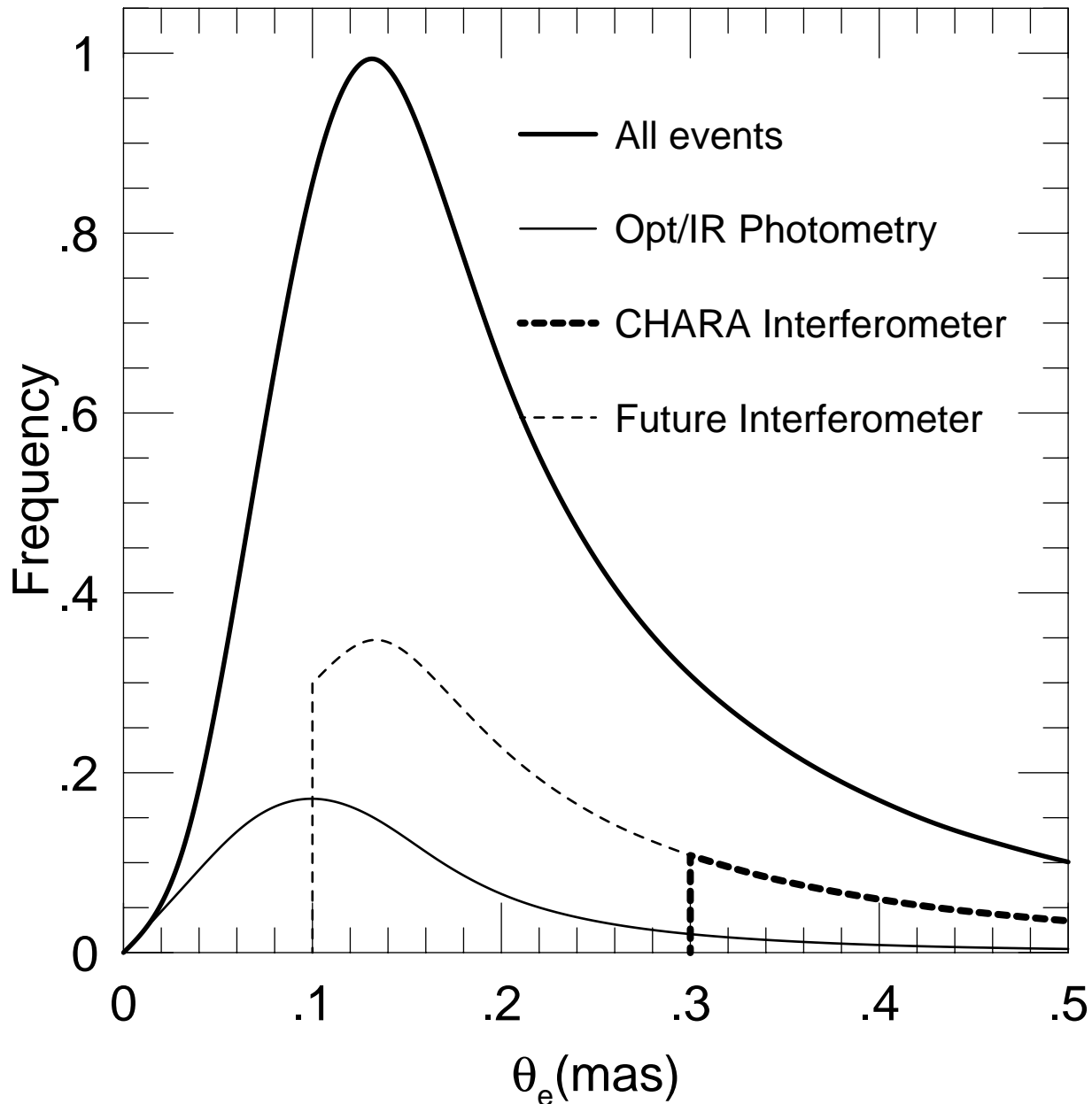


Figure 6. Bold solid curve is the expected distribution of Einstein radii θ_e toward the Galactic bulge based on the best fit power-law model of Han & Gould (1996a) (cf. Fig. 4). The fraction of giant-source events for which θ_e can be measured by optical/infrared photometry is shown as a solid curve. Note that this fraction $\propto \theta_e^{-1}$. For $\theta_e > 0.3$ mas, it is expected that θ_e can be measured for $\sim 35\%$ of events with the CHARA interferometer now under construction (bold dashed curve). A hypothetical interferometer with 3 times better resolution but the same magnitude limit is shown by a dashed curve.

to giants. Bulge giants have $V_0 < 16$, and in addition generally suffer several magnitudes of extinction. They are intrinsically brighter in the infrared ($H_0 < 13.5$) and in addition the extinction is typically low, $A_H < 0.5$. For the image splitting to be observed, the *fainter* image must be brighter than the magnitude limit. Thus, the half of giants with $H < 13$ require $\beta \lesssim 1/2$ and the remainder require

$\beta \lesssim 1/4$ [cf. eq. (3.6)]. I therefore estimate that $\sim 35\%$ of giant-source events with image separations > 0.6 mas (and hence Einstein rings $\theta_e > 0.3$ mas) could yield measurements of θ_e . This fraction is shown in Figure 6.

5.3. PROSPECTS

The instruments that would be required to make microlensing measurements of the MF are already being built or are the subject of active proposals. A parallax satellite was proposed as a MIDEX project, although it failed to win approval in the current round. The CHARA interferometer is scheduled for completion in 1999 (H. McAlister 1996, private communication). D. L. DePoy (1996, private communication) has designed an optical/infrared camera and a proposal to build it is now pending. Ultimately, one would want to place one of these cameras on each of several 1m class telescopes around the world in order to obtain 24 hour coverage of ongoing events. Two groups (PLANET and GMAN) are already monitoring ongoing microlensing events with conventional optical telescopes from sites encircling the globe.

From Figure 6 it is clear that even with all this equipment in place it would be possible to measure masses for only $\sim 15\%$ of giant-star events. However, interferometric technology is advancing at rapid rate. A factor ~ 3 improvement in resolution would allow one to measure the lens masses for $\sim 35\%$ of events and moreover would produce a representative sample of lenses, that is one with only modest (and hence easily corrected) selection bias (see Fig. 6).

6. Mass Function of the LMC

As discussed in the introduction, the microlensing observations toward the LMC are aimed primarily at discovering MACHOs in the Galactic halo. Inevitably, however, there will be some microlensing by stars in the Galactic disk, Galactic spheroid (stellar halo), and the LMC itself. To date, about eight candidate events have been reported by MACHO and two by EROS. Assuming that all these events are real, this rate implies an “optical depth” (probability that a given star is lensed at any given time) of $\tau \sim 2 \times 10^{-7}$. Star counts place strong constraints on the contribution to τ from luminous stars in the Galactic disk (Gould et al. 1996) and spheroid (Mould 1996; Flynn, Gould, & Bahcall 1996). On the other hand, Sahu (1994a,b) has argued that the majority of the events come from LMC stars. Although this is contested (Gould 1995b), one of the eight MACHO candidates is almost certainly in the LMC (Alcock et al. 1996c). The reason this is known is that the event is a binary lens with two “caustic crossings”. For such events it is possible to measure θ_e using a variant of the method discussed in § 5.2. One can

then determine the proper motion $\mu = \omega\theta_e$ which turns out to be consistent with the low values expected for LMC lenses, but is much too low for closer lenses.

To use microlensing to measure the LMC MF, one must first isolate a subsample of all events which are due to LMC lenses. One could do this with satellite observations of the type described in § 5.1. For LMC stars with e.g., $M \sim 0.3 M_\odot$, $D_{\text{ls}} \sim 1$ kpc, one finds $\tilde{r}_e \sim 75$ AU. Hence, LMC events would be recognized as those with $\Delta x = d_{\text{sat}}/\tilde{r}_e \ll 1$. However, given reasonable satellite design parameters (e.g., Boutreux & Gould 1996), it is likely that Δx would only be shown to be consistent with zero, not actually measured. Thus there would be no additional information from the parallax measurement beyond that the lens was in the LMC. Thus, the measurement of the MF is substantially more difficult for the LMC than the bulge, not only because there is a lower event rate, but because there is less information for each event measured.

7. Mass Function of M31 from Pixel Lensing

It has proven difficult to measure the MF even in the solar neighborhood, so the possibility of measuring the MF of the M31 bulge might seem remote at best. In fact, rapid progress is already being made.

The problem with doing lensing experiments toward the M31 bulge is that none of the stars are resolved. Instead, each pixel contains dozens or hundreds of bright stars and it is therefore impossible to measure the individual flux from any one of them. Recall from equation (3.10), however, that what is of interest is not the flux from the star, but the difference in flux from its unmagnified state. Crotts (1992) and Baillon et al. (1993) pointed out that this can be measured by monitoring the time dependence of the pixel counts. Both groups have initiated pixel lensing searches toward M31 and have achieved impressive initial results.

To understand pixel lensing, consider two images taken in identical seeing, with identical exposure times and atmospheric extinction, and perfectly aligned. One image is taken before and one during the lensing event. If the two images are subtracted, the difference image will look like a blank patch of sky containing a single stellar point spread function (PSF), with total flux $F = F_0(A - 1)$, exactly as in equation (3.10). One then constructs a light curve just as one would do in ordinary “classical” lensing.

Of course the seeing et cetera is never identical, so pixel lensing seems to many to be a hopeless illusion. However, it is possible to convolve images to the same seeing, to align them photometrically and geometrically, and to obtain difference images very much like those described. Both groups have used variations on this



Figure 7. Detection of variable stars in M31 using pixel-lensing techniques (Tomaney & Crotts 1996). (a) An R band reference image of M31 is constructed from 20 800 s integrations taken in $\sim 1''$ seeing between 20 Nov 1995 and 3 Dec 1995. The field is an $85''$ (256 pixel) square which is $400''$ from the center of M31 along the far minor axis. It has mean surface brightness $R \simeq 20 \text{ mag arcsec}^{-2}$. The large scale gradient has been removed in this display. Most of the variation is due to surface brightness fluctuations rather than individual stars. The bright object at the far right and $\sim 20''$ from the bottom is probably a globular cluster. From work to be published by Tomaney & Crotts (1996). Reproduced with permission.

technique to find large numbers of variable stars. In particular, Tomaney & Crotts (1996) have produced a spectacular difference image (reproduced as Fig. 7) in which the variables appear as positive and negative PSFs. It is not yet possible to confirm microlensing in these studies because of an inadequate baseline, but it

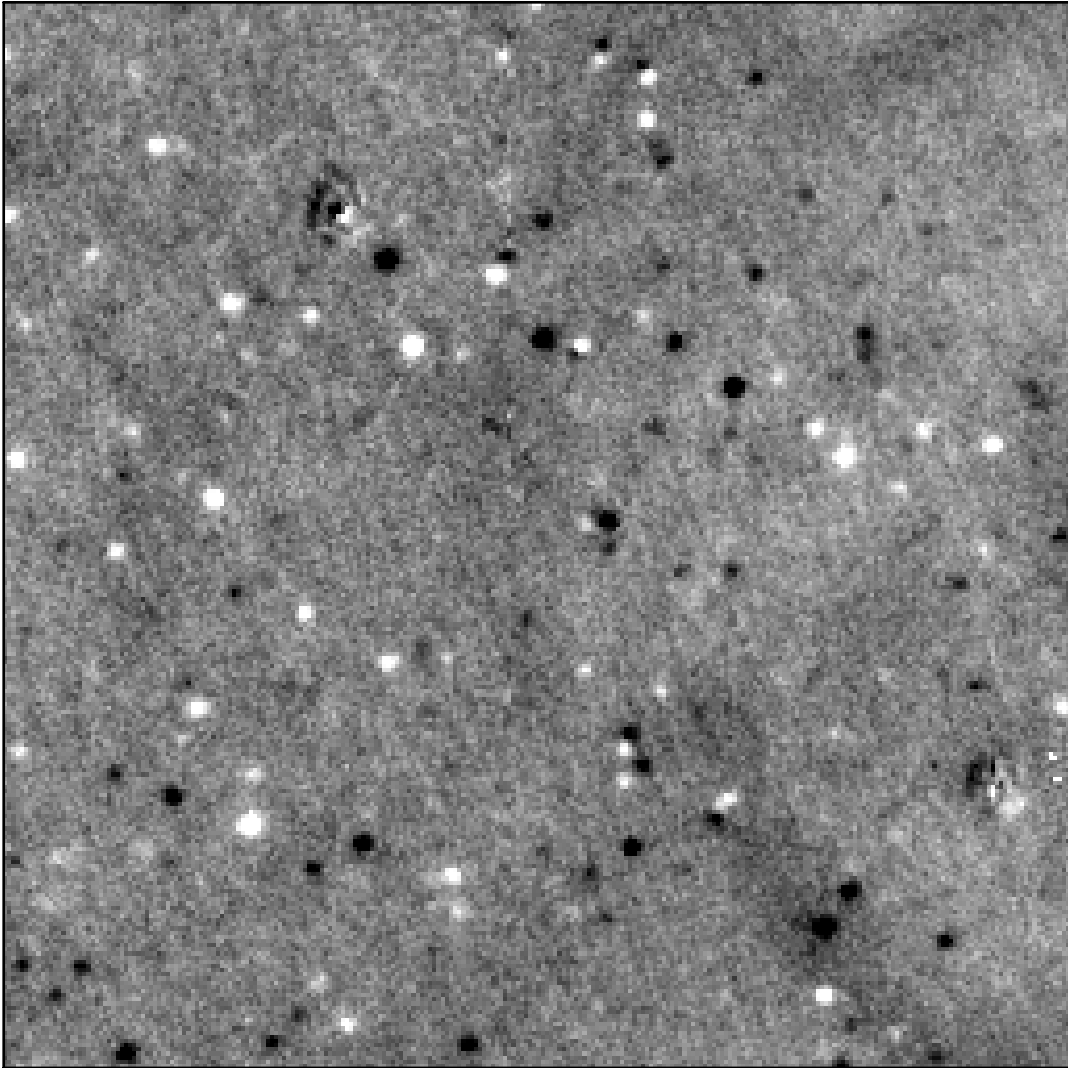


Figure 7. (b): The residuals formed by subtracting the reference image 7(a) from an image constructed from 10 800 s exposures taken on 21 Oct 1995 in $1''.2$ seeing after photometric and geometric registration and after convolving the reference image to bring it to the same seeing. Images (a) and (b) are shown at the same stretch. The bright and dark circles are PSF-shaped residual fluxes which are positive and negative respectively. The brightest flux differences correspond to $R \sim 21$ and the faintest to $R \sim 23$. While most of the objects seen in this difference image are undoubtedly variable stars, the image demonstrates that the pixel-lensing technique is viable and should be able to detect variation due to microlensing. From work to be published by Tomaney & Crofts (1996). Reproduced with permission.

should be possible in the near future.

What can be learned about the M31 MF from pixel lensing? For the foreseeable future, the only information available for most events will be the time scale, t_e .

Even the time scale can be difficult to recover for those events in which a very faint star is highly magnified ($\beta \ll 1$). In this case,

$$F = F_0(A - 1) \rightarrow \frac{F_{\max}}{[1 + (t - t_0)^2/t_{\text{eff}}^2]^{1/2}}, \quad (7.1)$$

where $F_{\max} \equiv F_0/\beta$ and $t_{\text{eff}} \equiv \beta t_e$. Since t_e does not appear in the limiting form (7.1) of the flux, it cannot generally be measured for these events. Nevertheless, if the signal-to noise ratio of the event is sufficiently high ($S/N \gtrsim 80$), then there is enough information to distinguish equation (3.10) from its limiting form (7.1). In these cases, it is possible to measure the time scale, just as it is for Galactic events (Gould 1996). Such high S/N events can occur in M31 either because the source star is relatively bright or the impact parameter β is small (Colley 1995; Han 1996). Han (1996) estimates that t_e can be measured for ~ 10 events per year assuming a modest dedicated experiment. Thus, pixel lensing will allow a statistical determination of the M31 MF of the type described in § 4. In particular, one can test whether the M31 bulge MF is consistent with the more accurately determined MF of the Galactic bulge.

What are the prospects for measuring θ_e and \tilde{r}_e for M31 lenses? Han & Gould (1996b) find that θ_e can be measured from finite-size effects (cf. § 5.2) for $\lesssim 1$ event per year. Moreover, $\tilde{r}_e \sim 10^3$ AU, so parallax measurements are out of the question for the near term.

In addition to obtaining information on the M31 MF, one would also find out about the LF. Recall from equation (3.10) that a microlensing light curve is a function of 4 parameters, including the source flux F_0 . This quantity is then measured in all events with good enough signal to noise to determine the time scale, estimated above at ~ 10 per year. Normally one does not think of microlensing as a way to determine the brightness of stars because it is so much easier to directly measure their flux. However, the stars in the M31 bulge are not resolved, so pixel lensing may be the only way to measure their flux and so determine the LF (Gould 1996).

8. Pixel Lensing of M87

There are several good reasons to search for microlensing in M87, the giant elliptical in the core of the Virgo cluster. First, a significant fraction of the halo of the Virgo cluster might well be made of MACHOs. Preliminary results of microlensing searches toward the LMC seem to indicate that $\gtrsim 20\%$ of the dark halo inside the LMC is composed of MACHOs (Alcock et al. 1993, 1995b, 1995d, 1996a, 1996c; Aubourg et al. 1993, 1995, Ansari et al. 1996). That is, the baryonic component of the Milky Way halo appears to be at least as massive as the visible baryons in the disk and bulge. One might imagine that half the available baryons formed MACHOs early in the Galaxy's history and the other half settled into a proto-disk and proto-bulge. Now consider a Milky Way-like galaxy forming on the edge of the Virgo cluster. It has time to form its MACHOs, but before the proto-disk can start forming stars, the galaxy falls into the cluster center and is stripped of its remaining gas by the intra-cluster medium. The MACHOs would then continue in their orbits, either as a relatively coherent dark galaxy or as a diffuse collection of Virgo halo objects. Either way, these objects would give rise to pixel lensing events of M87 (Gould 1995f). Second, M87 is a giant elliptical galaxy, and its stellar population could differ radically from those of the Galaxy and M31. Pixel lensing could test for such differences.

Unfortunately, pixel lensing increases in difficulty as the fourth power of the distance of the target galaxy. Two identical galaxies at different distances, d_1 and d_2 , will have the same surface brightness S . If observed from the same telescope, a resolution element Ω_{psf} will contain the same amount of flux, $S\Omega_{\text{psf}}$. Thus the photon noise will be the same for measurements of the same duration, Δt . On the other hand, the flux from a typical lensing event will be lower by a factor $(d_2/d_1)^{-2}$. Hence the ratio of the signal to noise (S/N) for the two galaxies is

$$\frac{(S/N)_2}{(S/N)_1} = \left(\frac{\Delta t_2}{\Delta t_1}\right)^{1/2} \left(\frac{d_2}{d_1}\right)^{-2}. \quad (8.1)$$

This implies that to reach more distant galaxies requires longer exposure times by $\Delta t \propto d^4$, or telescopes with proportionately larger apertures.

Another approach is increased resolution. Dedicated observations with *HST* would yield $\sim 18f$ Virgo cluster halo events and another ~ 3 events from M87 stars per day (Gould 1995f). Here f is the fraction of the Virgo halo composed on MACHOs. The two populations could be distinguished, at least statistically, because they would have different angular distributions.

9. Star Formation History of the Universe

Only a few years ago, measurements of the MF were restricted to stars in the “solar neighborhood”, the nearest 10s of pc. Today, it is already possible to probe not only distant parts of our own Galaxy, but even M87 at 10s of Mpc. Nevertheless, from a cosmological point of view the Virgo cluster is still the “solar neighborhood”. In Table 1, M87’s redshift z is still written in scientific notation. Will it ever be possible to determine the MF at such large distances that they represent different epochs in the history of the universe?

TABLE 1

Summary of Probes of The Stellar Mass Function

Method	Star Field	z
Parallax	10 pc from Sun	2×10^{-9}
Ground Photometry	100 pc from Sun	2×10^{-8}
HST Photometry	3 kpc from Sun	7×10^{-7}
Microlensing	MW Bulge and Disk	2×10^{-6}
Pixel Lensing	M31 Bulge	2×10^{-4}
Pixel Lensing	M87	4×10^{-3}

Actually, this may not be so difficult as it would first appear. There are 100 quasars to $B = 22$ per square degree. One could monitor these for gravitational lensing over say 10,000 deg². That would be 10⁶ quasars. The rate, Γ , at which known stars in galaxies would generate events is $\Gamma \sim 20 \text{ yr}^{-1}$. If the density of MACHOs (in or out of galaxies) were $\Omega_{\text{MACHOs}} \sim 1\%$, these would generate an additional $\Gamma \sim 200 \text{ yr}^{-1}$. The stellar events would typically last $\sim 10 \text{ yr}$, while the MACHO events would last $\sim 3 \text{ yr}$ (Gould 1995e). Because the events do last several years, it would be sufficient to monitor the quasars only several times per year. In fact it would be unnecessary even to identify the 10⁶ quasars. The 10,000 square degrees could be monitored with say a 4 square degree field on a 1 or 2 m telescope. Lensed quasars would be found by the same technique used in pixel lensing searches (see Fig. 7). The visible disks of galaxies cover about 1% of the sky and hence 1% all quasars lie behind these disks (Gould 1995c). If quasars in this subsample could be identified, it might be advantageous to monitor them more carefully.

What could be learned about stars in such a survey? First, the star formation history of the universe. If most stars formed before the epoch of quasars, then the optical depth to $z = 4$ quasars would be much higher than to $z = 1$ quasars, because the path length to the former would be densely populated with stars. On the other hand, if most stars formed at $z < 1$, then the distant quasars would have only a slight advantage in optical depth (Gould 1995e).

Second, one could learn, at least statistically, about the MF. Measuring the mass of individual lensing stars would be more difficult, although even this would be possible given a sufficient investment. For most stars, or at least the stars in galaxies, one could identify the host galaxy by following up the detection with deep imaging. Once the redshift of the galaxy were measured, one would have two measurements (distance and time-scale of the event) against three unknowns (the mass, distance, and transverse speed). In other words, the mass could be statistically estimated by assuming a distribution of transverse speeds of galaxies. It is in fact possible to measure the scale of the transverse speeds from the monitoring experiment by comparing the lensing rate toward quasars in directions parallel and perpendicular to the Sun's motion relative to the microwave background. But it is also possible to measure the transverse velocities of the lensing stars themselves, provided that one observes the event simultaneously from a satellite in a Neptune-like orbit (Gould 1995c). Such parallax measurements would be very similar to the measurements proposed for Galactic lensing events (Gould 1994b, 1995a) but on a much larger scale.

In fact, the first confirmed microlensing by a star was discovered not in our Galaxy but in Huchra's Lens (in front of qso 2237+0305) (Irwin et al. 1989; Corrigan et al. 1991). While only at $z = 0.04$, this serendipitous discovery may one day be regarded as the first step toward a measurement of the star-formation history of the universe.

One might wonder how one could distinguish genuine quasar microlensing events from ordinary quasar variations. In fact, this is not difficult in principle: spectroscopic follow up would reveal a light echo in the broad line region of any variation coming from the continuum. No such effect would be seen for microlensing. Unfortunately, the telescope time necessary to follow up all variations among 10^6 quasars would be prohibitive. However, in the original survey, one could identify a subset of relatively quiescent quasars or, more to the point, eliminate quasars that showed too much variation. Whether such a population of quiescent quasars exists is not presently known, but is likely to be determined as a by-product of large scale supernova searches to be carried out over the next few years.

I should add that the various proposals envisaged in §§ 8 and 9 differ dramatically in terms of resource requirements. A dedicated quasar variability search is the

same order of project as the MACHO searches that are now being undertaken by several groups. Dedicated *HST* observations of M87 would be similar in scope to the Hubble Deep Field (HDF) observations and hence would require either Director’s Discretionary Time (as with HDF) or at least very broad community support. On the other hand, a 1 m telescope in a Neptune-like orbit would be on the general scale of the most ambitious space-science projects, like *HST* itself.

10. Planet Searches

Microensing can be a powerful tool for studying planets as well as stars. Once a microensing event is under way, one can monitor the event to search for the short ($\lesssim 1$ day) perturbations characteristic of a planet. This in fact is the primary motivation of the two lensing follow up networks, PLANET (Albrow et al. 1996) and GMAN (Pratt et al. 1996).

Microensing searches for planets were first suggested by Mao & Paczyński (1991) who analyzed these events as the low mass limit of binary-lens microensing. Binary microensing is far more complicated than point-mass microensing. In particular, the light curves do not in general resemble a superposition of two point-mass curves of the type described by equation (3.7).

Planetary lensing is somewhat simpler than binary lensing because it can be described by a fourth order equation which can be solved analytically, rather than a fifth order equation which cannot (Gould & Loeb 1992). Nevertheless, a full treatment of planetary lensing is beyond the scope of the present review. For a large fraction of planetary lensing events, however, the light curve does in fact qualitatively resemble a superposition of two light curves. The primary light curve has time scale t_e and the perturbing light curve has duration $t_p \sim (m/M)^{1/2}t_e$, where M and m are the masses of the lensing star and its planet respectively. The planetary perturbation is shorter than the main event because the planet has a proportionately smaller Einstein ring, $\theta_p = (m/M)^{1/2}\theta_e$. This picture, while considerably oversimplified, does permit one to understand what can be learned from planetary microensing events.

One must distinguish between two classes of planetary lensing events, depending on whether the planet Einstein radius θ_p is bigger or smaller than the stellar radius θ_* . For an average giant source ($\theta_* = 22r_\odot/R_0$), and a planetary system at $D_1 \sim 6$ kpc toward the bulge, the boundary between these regimes is at $m \sim 85 M_\oplus$ where M_\oplus is the mass of the Earth.

Consider first the case of $\theta_p > \theta_*$, the “Jupiters”. Naively, the fraction of events where the planet causes a recognizable perturbation is $\sim \theta_p/\theta_e = (m/M)^{1/2}$, or $\sim 3\%$ for a Jupiter in orbit around a solar type star. In fact, a more detailed

analysis shows that the lensing star actually stretches the Einstein ring of the planet so that the fraction of noticeable events is much higher, $\sim 17\%$ for a Jupiter (Gould & Loeb 1992). One can measure two quantities in this case, the ratio of the masses of the planet to the star and the projected separation of the planet from the star in units of the Einstein ring. The mass ratio is determined from the measured ratio of time scales $m/M = (t_p/t_e)^2$, and the projected separation in units of the Einstein ring is simply the value of x when the planetary event occurs. Since the mass and Einstein radius of the parent star can be estimated to within a factor of $\sim 2\text{--}3$, the mass and separation of the planet are known equally well. If there is additional information such as \tilde{r}_e from parallax (§ 5.1), θ_e (§ 5.2), or a measurement of the spectral type of the parent star (Gould & Loeb 1992; Buchalter, Kamionkowski, & Rich 1996), then the mass and separation can be further constrained or precisely specified.

The case of $\theta_p < \theta_*$ is rather different. First, the probability of a planetary event scales not with θ_p but with θ_* . This means that no matter how small the planet, there is a probability $\sim \theta_*/\theta_e$ that a planetary event will take place (assuming of course that the star has a planet in the neighborhood of the Einstein ring). For an $M = 0.5 M_\odot$ star at 6 kpc lensing an average giant, this is $\sim 3\%$, small but not negligible given that an aggressive search toward the bulge could detect ~ 100 giant-source lensing events per year (Gould 1995d). In fact, microlensing is the only known technique for detecting Earth-mass planets from the ground. Note that the sensitivity of the survey could be increased somewhat by also monitoring the more numerous (but much smaller) turn off stars in the bulge.

However, a second major effect when $\theta_p < \theta_*$ is that the maximum size of the perturbation is only $\sim 2(\theta_p/\theta_*)^2$, or $\sim 1.4\%$ for an Earth-mass planet with the above geometry. The events would last for the time it took for the planet to cross the source star, typically ~ 10 hours. It is not difficult to detect $\sim 1\%$ variation of a bright giant which is monitored continuously. However, since the detections are not repeatable, one might well question whether any particular event was real, or whether it resulted from intrinsic variation or just an instrument glitch. In order to confirm events on a routine basis, it is therefore important to make simultaneous optical/infrared images using a dichroic beam splitter such as has been proposed by D. L. DePoy (1996 private communication). Not only would such observations have the important feature of redundancy, but limb darkening would generate a characteristic color variation during the planetary perturbation which would unambiguously distinguish it from any other possible cause (Gould & Welch 1996).

A third feature of small-mass planet events is that it is almost always possible to measure θ_p , because the planet almost always transits the image of the star. This means that the mass is generally better constrained for these events. Moreover, if

there is a parallax measurement, the mass can be determined precisely.

11. Summary

The original object of microlensing surveys was to find the dark matter in the halo of the Milky Way (Paczynski 1986) and other galaxies (Crotts 1992; Baillon et al. 1993; Gould 1993). However, even before the surveys got started, they began to expand their horizons to become probes of visible as well as dark matter (Paczynski 1991; Griest et al. 1991). Once underway, the successes of the microlensing surveys inspired many ideas for extracting additional information from the data, in particular methods for constraining or measuring the masses of the lenses. With the development of these new techniques, microlensing promises to provide a powerful probe of the stellar MF and a method for mapping out the distribution of sub-stellar objects including planets. Unlike traditional approaches to measuring the MF, microlensing is not restricted to the solar neighborhood, or even the Galaxy, Local Group, or Local Supercluster. Microlensing is already giving hints of an unexpected population of low mass stars in our Galaxy, and may yet tell us something about stars at the edge of the universe.

Acknowledgements: I would like to thank K. Griest, G. Newsom, J. Rich and K. Sahu for making many valuable suggestions and to extend special thanks to A. Tomaney and A. Crotts for giving permission to use their spectacular difference image of M31 in advance of publication. This work was supported in part by grant AST 94-20746 from the NSF.

REFERENCES

- Alard, C. 1996, in Proc. IAU Symp. 173 (Eds. C. S. Kochanek, J. N. Hewitt), in press (Kluwer Academic Publishers)
- Alard, C., Mao, S., & Guibert, J. 1995, A&A, L17
- Albrow, M., et al. 1996, in Proc. IAU Symp. 173 (Eds. C. S. Kochanek, J. N. Hewitt), in press (Kluwer Academic Publishers)
- Alcock, C., et al. 1993, Nature, 365, 621
- Alcock, C., et al. 1995a, ApJ, 445, 133
- Alcock, C., et al. 1995b, ApJ, 449, 28
- Alcock, C., et al. 1995c, ApJ, 454, L125
- Alcock, C., et al. 1995d, Phys. Rev. Lett., 74, 286
- Alcock, C., et al. 1996a, ApJ, submitted
- Alcock, C., et al. 1996b, ApJ, submitted
- Alcock, C., et al. 1996c, ApJ, in preparation
- Alcock, C., et al. 1996d, ApJ, in preparation
- Ansari, R., et al. 1996, A&A, in press
- Aubourg, E., et al. 1993, Nature, 365, 623
- Aubourg, E., et al. 1995, A&A, 301, 1
- Bahcall, J. N., Flynn, C., Gould, A. & Kirhakos, S. 1994, ApJ, 435, L51
- Baillon, P., Bouquet, A., Giraud-Héraud, Y., & Kaplan, J. 1993, A&A, 277, 1
- Bessel, M. S. & Stringfellow, G. S. 1993, ARAA, 433
- Boutreux, T., & Gould, A. 1996, ApJ, 462, 000
- Buchalter, A., Kamionkowski, M., & Rich, R. M. 1996, ApJ, submitted
- Colley, W. N. 1995, AJ, 109, 440
- Corrigan, R. T., et al. 1991, AJ, 102, 34
- Crotts, A. P. S. 1992, ApJ, 399, L43
- Flynn, C., Gould, A., & Bahcall, J. N. 1996, ApJL, submitted
- Gaudi, B. S., & Gould, A. 1996, ApJ, submitted
- Gould, A. 1992, ApJ, 392, 442
- Gould, A. 1993, ApJ, 404, 451
- Gould, A. 1994a, ApJ, 421, L71

- Gould, A. 1994b, ApJ, 421, L75
- Gould, A. 1995a, ApJ, 441, L21
- Gould, A. 1995b, ApJ, 441, 77
- Gould, A. 1995c, ApJ, 444, 556
- Gould, A. 1995d, ApJ, 447, 491
- Gould, A. 1995e, ApJ, 455, 37
- Gould, A. 1995f, ApJ, 455, 44
- Gould, A. 1996, ApJ, submitted
- Gould, A., Bahcall, J. N. & Flynn, C. 1996, ApJ, 465, 000
- Gould, A., & Loeb, A. 1992, ApJ, 396, 104
- Gould, A., & Welch, R. L. 1996, ApJ, 464, 000
- Griest, K. et al. 1991, ApJ, 372, L79
- Han, C. 1996, ApJ, submitted
- Han, C., & Gould, A. 1995, ApJ, 447, 53
- Han, C., & Gould, A. 1996a, ApJ, 467, 000
- Han, C., & Gould, A. 1996b, ApJ, submitted
- Han, C., Narayanan, V. K., & Gould, A. 1996, ApJ, 461, 587
- Henry, T. J. & McCarthy, D. W. 1993, AJ, 106, 773
- Hog, E., Novikov, I. D., & Polnarev, A. G. 1995, A&A, 294, 287
- Irwin, M. J., Webster, R. L., Hewett, P. C., Corrigan, R. T., & Jedrzejewski, R. I. 1989, AJ, 98, 1989
- Jetzer, P. 1994, ApJ, 432, L43
- Kiraga, M. & Paczyński, B. 1994, ApJ, 430, 101
- Kirkpatrick J. D., McGraw, J. T., Hess, T. R., Liebert, J. & McCarthy, D. W., Jr. 1994, ApJS, 94, 749
- Liouville, J. 1837, Journal de Mathématiques Pures et Appliquées, 2, 16
- Loeb, A. & Sasselov, D. 1995, ApJ, 449, L33
- Mao, S. & Paczyński, B. 1991, ApJ, 388, L45
- McAlister, H. A. et al. 1994, SPIE, 2200, 129
- McAlister, H. A., Bagnuolo, W. G., ten Brummelaar, T., Hartkopf, W. I., & Mason, B. D. 1995, The CHARA Array as an ASEPS Resource, Technical Report No. 18, (Center for High Angular Resolution Astronomy, Georgia State University: Atlanta)

- Misner, C. W., Thorne, K. S., & Wheeler, J. A. 1973, *Gravitation*, (San Francisco: Freeman)
- Mould, J. 1996, *PASP*, 108, 35
- Nemiroff, R. J. & Wickramasinghe, W. A. D. T. 1994, *ApJ*, 424, L21
- Paczynski, B. 1986, *ApJ*, 304, 1
- Paczynski, B. 1991, *ApJ*, 371, L63
- Paczynski, B. 1996, *ARAA*, submitted
- Pratt, M., et al. 1996, in *Proc. IAU Symp. 173* (Eds. C. S. Kochanek, J. N. Hewitt), in press (Kluwer Academic Publishers)
- Refsdal, S. 1966, *MNRAS*, 134, 315
- Reid, I. N., Hawley, S. L., & Gizis, J. E. 1995, *AJ*, 110, 1838
- Reid, I. N., Tinney, C. G., & Mould J. 1994, *AJ*, 108, 1456
- Roulet, R. & Mollerach, S. 1996, *Physics Reports*, submitted
- Sahu, K. C. 1994a, *Nature*, 370, 275
- Sahu, K. C. 1994b, *PASP*, 106, 942
- Scalo, J. M. 1986, *Fund. Cos. Phys.*, 11, 1
- Schneider, P., Ehlers, J., & Falco, E. E. 1992, *Gravitational Lenses* (Berlin: Springer-Verlag)
- Stobie, R. S., Ishida, K., & Peacock, J. A. 1989, *MNRAS*, 238, 709
- Tomaney, A., & Crofts, A. P. S. 1996, in preparation
- Udalski, A., et al. 1994a, *Acta Astronomica* 44, 165
- Udalski, A., Szymański, M., Kaluzny, J., Kubiak, M., W., Mateo, M., & Krzemiński, W. 1994b, *ApJ* 426, L69
- Udalski, A., et al. 1994c, *ApJ* 436, L103
- Wielen, R., Jahreiss, H., & Krüger, R. 1983, *IAU Coll. 76: Nearby Stars and the Stellar Luminosity Function*, A. G. D. Philip and A. R. Upgren eds., p 163
- Witt, H. 1995, *ApJ*, 449, 42
- Witt, H., & Mao, S. 1994, *ApJ*, 430, 505
- Zhao, H. S., Spergel, D. N., & Rich, R. M. 1995, *ApJ*, 440, L13